

Supplementary Information for “A numerical investigation of dimensionless numbers characterizing meltpool morphology of the laser powder bed fusion process”

Kunal Bhagat, Shiva Rudraraju

Department of Mechanical Engineering, University of Wisconsin-Madison, Madison, WI, USA

Material properties and process variables

Material properties of various alloys and the corresponding AM process variables used in this work are listed here. These properties were collected from multiple sources in the literature. The properties of solid and liquid materials are averaged and dependence on the temperature is neglected.

Table 1: Average material properties for different alloys used to calculate input non-dimensional numbers of the thermo-fluidic model [21], [58], [63]

| Property | SS316 | Ti6Al4V | IN718 | AlSi10Mg | AZ91D |
|------------------------------------|------------------------|------------------------|------------------------|------------------------|------------------------|
| $\rho(\frac{kg}{m^3})$ | 7800 | 4000 | 8100 | 2670 | 1675 |
| $c(\frac{J}{kgK})$ | 490 | 570 | 435 | 890 | 1122 |
| $k(\frac{W}{mk})$ | 36.5 | 7.3 | 11.4 | 173.0 | 77.5 |
| $\mu(\frac{Kg}{ms})$ | 7.0×10^{-3} | 4.0×10^{-3} | 5.0×10^{-3} | 1.3×10^{-3} | 3.0×10^{-3} |
| $\frac{d\gamma}{dT}(\frac{N}{mK})$ | -4.00×10^{-4} | -2.63×10^{-3} | -3.70×10^{-3} | -3.5×10^{-4} | -2.13×10^{-4} |
| $\beta(\frac{1}{K})$ | 5.85×10^{-5} | 2.50×10^{-5} | 4.8×10^{-5} | 2.4×10^{-5} | 9.54×10^{-5} |
| $\kappa(m^2)$ | 5.56×10^{-13} |
| $L(\frac{J}{kg})$ | 2.72×10^5 | 2.84×10^5 | 2.09×10^5 | 4.23×10^5 | 3.73×10^5 |
| $T_s(K)$ | 1693 | 1878 | 1533 | 831 | 743 |
| $T_l(K)$ | 1733 | 1928 | 1609 | 867 | 868 |

Table 2: Chosen process conditions for different alloys used to calculate input non-dimensional numbers of the thermo-fluidic model

| Material | (Laser Power, Scan speed) (P, ν_p) |
|----------|---|
| SS316 | (70, 0.3), (80, 0.4), (90, 0.5), (100, 0.6) |
| | (110, 0.7), (110, 0.8), (110, 0.9), (110, 1.0) |
| | (65, 0.5), (75, 0.5), (85, 0.5), (95, 0.5) |
| Ti6Al4V | (15, 0.2), (25, 0.5), (35, 0.7), (45, 0.9) |
| | (40, 0.6), (40, 0.7), (40, 0.8), (40, 1.0) |
| | (35, 0.9), (40, 0.9), (45, 0.9), (50, 0.9) |
| IN718 | (20, 0.15), (30, 0.25), (40, 0.45), (50, 0.75), |
| | (45, 0.80), (45, 0.90), (45, 1.0), (45, 1.1) |
| | (53, 0.95), (55, 0.95), (58, 0.95), (60, 0.95) |
| AlSi10Mg | (75, 0.35), (85, 0.45), (95, 0.55), (105, 0.65) |
| | (100, 0.6), (100, 0.7), (100, 0.8), (100, 0.9) |
| | (90, 1.1), (95, 1.1), (100, 1.1), (110, 1.1) |
| AZ91D | (35, 0.25), (40, 0.30), (45, 0.35), (50, 0.45) |
| | (40, 0.30), (40, 0.40), (40, 0.50), (40, 0.60) |
| | (40, 0.60), (50, 0.60), (60, 0.60), (70, 0.60) |

Additional correlations of the dimensionless numbers

The influence of the Péclet number on advection transport in the melt pool for additional materials IN718 and AZ91D is shown in Figure 1, and the corresponding comparison of the five alloys considered in this work is given in Figure 2. The combined plot of aspect ratio with $Ma\hat{U}$ is given in the Figure 3. The melt pool aspect ratio and Marangoni number of IN718 and Ti6AL4V are similar magnitudes. Similarly, the melt pool aspect ratio and Marangoni number of AZ91D and AlSi10Mg are comparable. The influence of Stefan number on the melt pool volumes for IN718 and AZ91D is shown in Figure 4, and the corresponding comparison of the five alloys considered in this work is given in Figure 5. Influence of dimensionless heat absorbed on non-dimensional temperature gradient (G) for IN718 and AZ91D is shown in Figure 6.

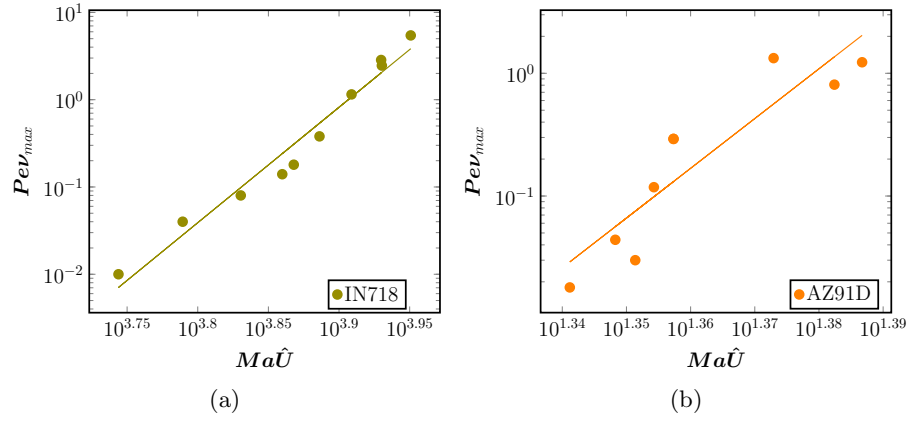


Figure 1: Measure of total advection measured as $Pe\nu_{max}$ vs surface tension based advection $Ma\hat{U} = a_0Ma + a_1MaE + a_2MaPe$ on a log-log scale for (1a) IN718 (1b) AZ91D, alloys.

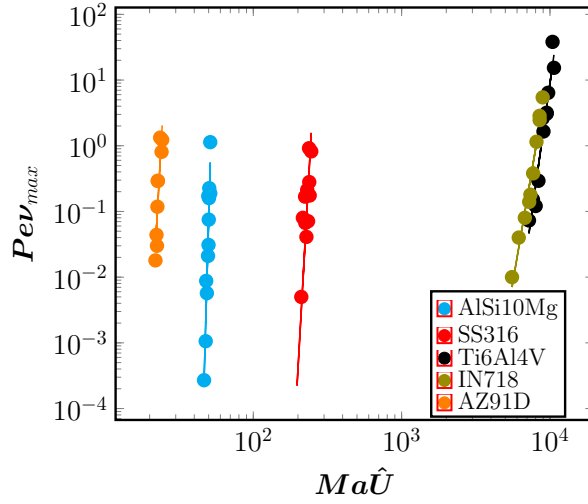


Figure 2: Measure of total advection measured as $\mathbf{Pe}\nu_{\max}$ vs surface tension based advection $\mathbf{Ma}\hat{\mathbf{U}} = a_0\mathbf{Ma} + a_1\mathbf{Ma}\mathbf{E} + a_2\mathbf{Ma}\mathbf{Pe}$, plotted on a log-log scale, for all the five alloys (AlSi10Mg, SS316, Ti6Al4V, IN718 and AZ91D) considered in this work.

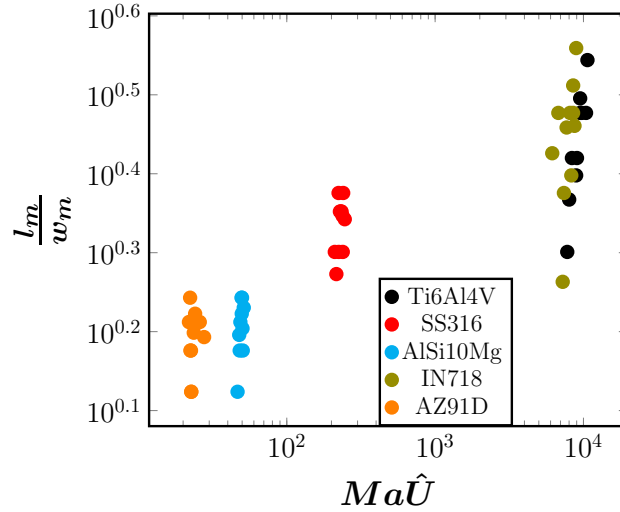


Figure 3: Correlation of the aspect ratio with $\mathbf{Ma}\hat{\mathbf{U}} = a_0\mathbf{Ma} + a_1\mathbf{Ma}\mathbf{E} + a_2\mathbf{Ma}\mathbf{Pe}$, plotted on a log-log scale, for all five alloys (Ti6Al4V, SS316, AlSi10Mg, IN718 and AZ91D) shown in a single plot to demonstrate clustering.

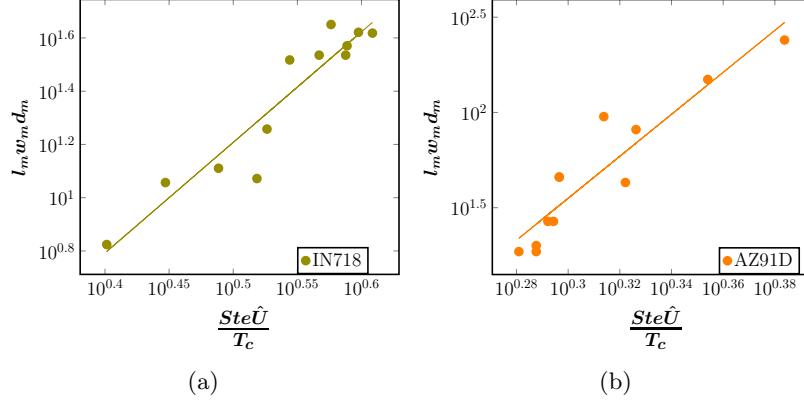


Figure 4: Correlation of the melt pool volume ($l_m w_m d_m$) with $\frac{Ste \hat{U}}{T_c} = a_0 \frac{Ste}{T_c} + a_1 \frac{Ste E}{T_c} + a_2 \frac{Ste Pe}{T_c}$, plotted on a log-log scale, for (4a) IN718, and (4b) AZ91D, alloys.

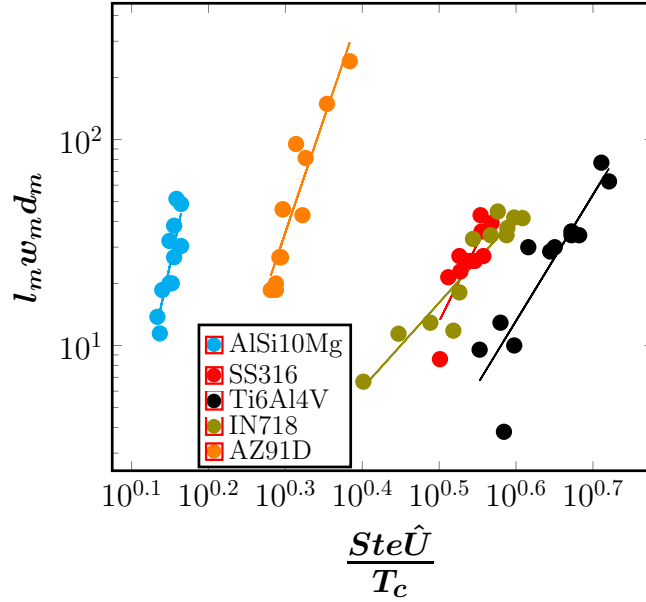


Figure 5: Correlation of the melt pool volume ($l_m w_m d_m$) with $\frac{Ste \hat{U}}{T_c} = a_0 \frac{Ste}{T_c} + a_1 \frac{Ste E}{T_c} + a_2 \frac{Ste Pe}{T_c}$, plotted on a log-log scale, for all the five alloys (AlSi10Mg, SS316, Ti6Al4V, IN718 and AZ91D) considered in this work.

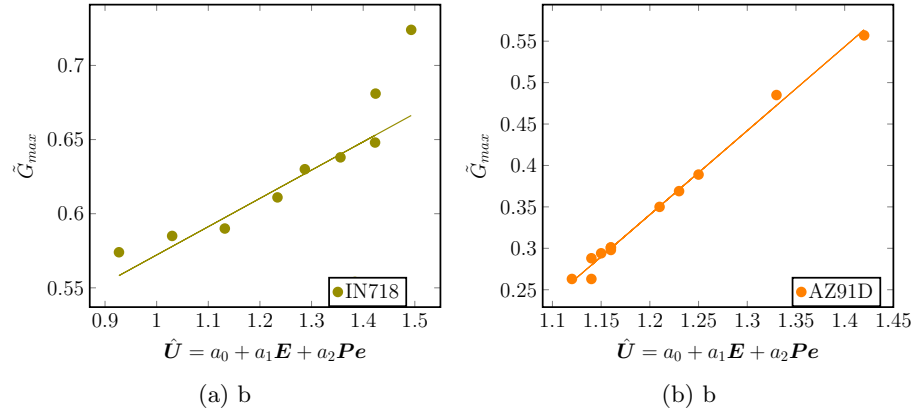


Figure 6: Dimensionless temperature gradient (G) with the \hat{U} for (6a) IN718 and (6b) AZ91D alloys.